Analytical Methods

ROYAL SOCIETY OF CHEMISTRY

MINIREVIEW

View Article Online
View Journal | View Issue

Check for updates

Cite this: *Anal. Methods*, 2023, **15**, 2709

Electroanalytical overview: the sensing of hydroxylamine

Prashanth S. Adarakatti, [ab] Robert D. Crapnell [a] and Craig E. Banks *[a]

Received 28th April 2023
Accepted 17th May 2023

DOI: 10.1039/d3ay00658a

rsc.li/methods

One of the principal raw ingredients used in the manufacturing of pharmaceuticals, nuclear fuel, and semiconductors is hydroxylamine, a mutagenic and carcinogenic substance, ranking high on the list of environmental contaminants. Electrochemical methods for monitoring hydroxylamine have the advantage of being portable, quick, affordable, simple, sensitive, and selective enough to maintain adequate constraints in contrast with conventional yet laboratory based quantification methods. This review outlines the most recent advancements in electroanalysis directed toward the sensing of hydroxylamine. Potential future advancements in this field are also offered, along with a discussion of method validation and the use of such devices in real samples for the determination of hydroxylamine.

1. Introduction to hydroxylamine

Hydroxylamine, NH_2OH, is an oxygenated form of ammonia often found within industrial and pharmaceutical processes, and semiconductor, chemical, and pharmaceutical industries.[1] Hydroxylamine is a well-known agent of mutation that is relatively toxic, causing injury and both physiological changes in plants, animals, and humans who come into contact with it.[2,3] The skin, eyes, different secretory systems, and breathing pathways can all get irritated by hydroxylamine. Moreover, exposure to hydroxylamine over a prolonged period can give rise to skin allergies as well as blood changes that can deplete glutathione and produce methaemoglobin, which over time can cause anaemia. Hydroxylamine is believed to be stable at a pH of 4 for a few hours, but at a pH of 7.8, it will only be stable for one hour. Determining hydroxylamine directly in environmental and biological samples is indeed challenging due to its fragility. There are no regulatory limits published by the US EPA

[a]*Faculty of Science and Engineering, Manchester Metropolitan University, Chester Street, Manchester M1 5GD, UK. E-mail: c.banks@mmu.ac.uk; Tel: +44 (0) 1612471196*

[b]*Department of Chemistry, SVM Arts, Science & Commerce College, Ilkal-587125, Karnataka, India*

Prashanth S. Adarakatti did his post graduation from P. C. Jabin Science College, Hubballi, India. He completed his Doctorate degree in 2017 from Central College, Bangalore University, India. Then he started his post-doctoral studies in the Indian Institute of Science (IISc), Bengaluru, India. He is working as Assistant Professor of Chemistry in SVM Arts, Science and Commerce College, ILKAL, affiliated to Rani Channamma University, Belagavi, Karnataka, India. Presently, he is working as a research associate in Manchester Metropolitan University, Manchester, UK under Prof. Craig E. Banks' supervision. To date he has published more than 50 original research articles and 10 book chapters. His research focuses on the development of electrochemical sensors and electroanalysis of energy materials.

Robert D. Crapnell achieved both his MChem and PhD from the University of Hull, United Kingdom, respectively, in 2014 and 2018. He is currently a senior research associate at Manchester Metropolitan University, United Kingdom. His research is predominantly focused on fundamental electrochemistry, additive manufacturing, sustainability, bespoke filament production and electrochemical and thermal biosensor development.

or WHO, but its permissible daily exposures limit for hydroxylamine is 2 μg day^{-1} as reported by the ICH M7 guideline.[4] There have been many methods employed in recent years to measure hydroxylamine, including flow-injection bi-amperometry,[5] high-performance liquid chromatography,[6] chemiluminescence,[7] spectrophotometry,[8] and gas chromatography.[9] In this minireview, we concentrate on using several modified electrodes and the electrochemical methods used to detect hydroxylamine species from various sample matrices.

2. Electrochemical based sensors for hydroxylamine

Table 1 overviews the endeavours directed toward the electroanalytical sensing of hydroxylamine, summarised in terms of the electrode material. We can observe that platinum, gold, glassy carbon (GC), carbon paste (CP), pencil graphite and screen-printed electrodes (SPEs) have all be utilised and report impressive dynamic ranges with low limits of detection (LOD) down to the nano-molar level. Herein we overview the most essential reports for the sensing of hydroxylamine.

The electrochemistry of hydroxylamine can occur *via* oxidation or reduction. For example, the electrochemical reduction has been studied at a dropping mercury electrode[10] and a rotating platinum electrode,[11] where the mechanism corresponds to:

$$NH_2OH + H_2O + 2e^- \rightarrow NH_3 + 2OH^- \quad (1)$$

It is reported that a copper electrode can undergo eqn (1) but it loses its activity rapidly,[12] but this can be overcome by using copper nanoparticles immobilised on a platinum electrode surface or through the use of platinum nanoparticles supported upon a copper electrode surface. In the latter configuration, it was utilised as a sensor towards the measurement of hydroxylamine which gave a linear range from 5 to 110 μM with a limit of detection (LOD) reported to 0.628 μM.

Of note, as presented within Table 1, most, if not all researchers prefer the electrochemical oxidation of hydroxylamine. The electrochemical oxidation of hydroxylamine is exemplified by understanding the cyclic voltammetry recorded using a 2-mercapto-4-methyl-5-thiazoleacetic acid (TAA) capped fused spherical gold nanoparticles (AuNPs) modified Au electrode; as shown within Fig. 1 as presented by Kannan and John.[13] The TAA-AuNPs were immobilized on a (3-mercaptopropyl)-trimethoxysilane (MPTS) sol–gel film, which was pre-assembled on a gold macroelectrode.[13] The cyclic voltammograms are presented for bare Au, Au/MPTS and Au/MPTS/TAA-AuNPs modified electrodes in 0.2 M PB solution (pH = 7.2) containing 0.5 mM HA. As shown (Fig. 1), the bare Au macroelectrode showed an electrochemical oxidation signal for hydroxylamine at +0.30 V (curve a), whereas no electrochemical oxidation wave was observed at Au/MPTS modified electrode (curve b) due to the formation of a compact MPTS sol–gel film on Au electrode. Note that the fused TAA-AuNPs modified electrode showed the electrochemical oxidation peak for HA at +0.20 V, in addition to a shoulder wave around +0.40 V (curve c). When compared to bare Au macroelectrode (curve a), the electrochemical oxidation peak potential of hydroxylamine was shifted to 100 mV less positive potential while the oxidation current was three times higher at the AuNPs modified electrode (curve c), which arises due to the larger surface area of the gold nanoparticles. The pK_a value of the hydroxylamine cation, is reported to be 5.9,[10] which showed only one electrochemical signal at pH 6 (<6), while in neutral or alkaline medium one additional electrochemical signal at more positive potential was observed (Fig. 1B). At pH greater than 5.9, hydroxylamine exists as non-protonated (NH_2OH) and protonated (NH_3OH^+) forms where the protonated form has been assumed to be less active.[14] Thus, it is assigned that the oxidation peak at +0.20 V to the non-protonated form of hydroxylamine and the shoulder wave around +0.40 V (curve d) to the electrochemical oxidation of protonated form. Similar electrochemical behaviour for hydroxylamine was recently reported at hybrid nickel–cobalt hexacyanoferrate modified electrode.[14] Furthermore, the oxidation of hydroxylamine at AuNPs modified electrode was found to be highly stable. The electrochemical oxidation mechanism of hydroxylamine, which is summarized within Fig. 1C is as follows:[13]

$$NH_2OH \rightarrow 1/2N_2O + 1/2H_2O + 2H^+ + 2e^- \quad (2)$$

Craig E. Banks holds a personal chair in nano- and electrochemical technology and has published over 600 papers and works on next generation screen-printed electrochemical sensing platforms as well the use of additive manufacturing in water splitting, sensor design, supercapacitors and battery development.

3. Glassy carbon electrode-based sensors

It can be seen through the inspection of Table 1, a glassy carbon electrode (GCE) as a supporting electrode has been used extensively as the basis of a hydroxylamine sensor. Electrocatalytic approaches have been reported, for example, liquid chromatography with amperometry has been used for the sensing of hydroxylamine and its *N*-mono-, *N*,*N*-di-, and *O*-substituted derivatives *via* a polymeric layer of cobalt phthalocyanine (CoPC)[15] which gave an LOD reported to 20 nM. Others have utilized alizarine red S (ARS) as the basis of a sensor for hydroxylamine,[16] of which the electrocatalytic signal is reported to be:

Table 1 An overview of the endeavours directed to the electroanalytical sensing of hydroxylamine[a]

Electrode material	Detection method	Dynamic range	Electrode modification	Limit of detection	Sample medium	Reference
Platinum microelectrode	DPV	25 μM–2.5 mM	NA	15 μM	N/A	65
Gold macroelectrode	Amperometry	17.5 nM–22 mM	Fused TAA-AuNPs/MPTS/Au NPs	0.39 nM	Ground water	13
GCE	Amperometry	0.1 μM–6 mM	PEDOT/GO	0.04 μM	Tap water	66
GCE	DPV	1–10, 10–100 μM	Indenedione derivative/MWCNTs	0.8 μM	Tap and well water	67
GCE	LC	2×10^{-8} M–5×10^{-6} M	Cobalt phthalocyanine	20 nM	N/A	15
GCE	Amperometry	2.0×10^{-5}–1.0×10^{-2} M	Nickel-cobalt hexacyanoferrate	2.3×10^{-7} M	N/A	14
GCE	DPV	1–500; 500–18 000 μM	Au NPs/polypyrrole	0.2 μM	N/A	68
GCE	Chronoamperometry	10–800 μM	Alizarine red S	7.2 μM	Drinking and well water	16
GCE	DPV	1–300 μM	C_{60}–CNTs/ionic liquid	28 nM	Top and auxiliary cooling water	24
GCE	Amperometry	11.8–2900.7 μM	Chlorogenic acid/MWCNT	1.4 μM	Drinking and tap water	69
GCE	Amperometry	0.4–19 000 μM	ZnO/MWCNTs	0.12 μM	Distilled water	54
GCE	Amperometry	0.5–400 μM	Baicalin/MWCNTs	0.1 μM	Tap water	21
GCE	Amperometry	1–5000 μM	PEDOP/MWCNTs-Pd NPs	0.22 μM	N/A	70
GCE	CV	0.2–150 μM	NiHCF/GO-CNTs	0.08 μM	N/A	71
GCE	Amperometry	3.0–69.8 μM, 69.8–915.2 μM	Anthio-quinazoline/MWCNTs	0.83 μM	Tap and drinking water	18
GCE	Amperometry	1.5 μM–2 mM	Prussian Blue/MWCNTs		N/A	17
GCE	DPV	0.45–1200 μM, 1200–19000 μM	Au NPs/polypyrrole	0.045 μM	Distilled water	72
GCE	LSV	0.5–1100 μM, 1100–19 000 μM	Pt NPs/choline film	0.07 μM	Ground and cooling water	73
GCE	LSV	0.5–1100 μM	Pt NPs/polypyrole	0.08 μM	Distilled water	74
GCE	SWV	4.0×10^{-7}–6.75×10^{-4} M	1-Benzyl-4-ferrocenyl-1*H*-[1,2,3]-triazole/CNTs	28.0 nM	Tap, drinking and river water	75
GCE	Amperometry	5.8–733.8; 733.8–2933.8 μM	CuTCPP/pOMC composites	0.8 μM	Tap water, lake water	76
GCE	Amperometry	5–1000 μM	Cobalt–RuO_2 NPs	2.4 μM	Ground and pond water	77
GCE	DPV	0.01–20 μM	AuNPs/MMPF-6(Fe)	4 nM	Tap and river water, PAM injection, oxyurea capsule	25
GCE	DPV	10–1000 μM	Fe_3O_4	0.65 μM	N/A	78
GCE	Amperometry	1–100 μM, 100–1000 μM	Cu^{2+}/curcumin/SWCNTs	0.019 μM	Hydroxyurea, pralidoxime iodide (PAM)	22
GCE	Amperometry	10–100 μM	Au NPs/CTAB/GO	3.5 μM	Tap and lake water	79
GCE	Amperometry	0.1–10 μM, 10–1000 μM	Brucine/SWNTs	0.021 μM	Hydroxyurea, pralidoxime iodide (PAM)	80
GCE	DPV	0.45–69.4 μM, 69.4–833.3 μM	OAgNPs	0.1 μM	Tap and drinking water	26
GCE	DPV	75–8250 μM	$CuCo_2O_4$	0.65 μM	Waste and lake water	23
GCE	DPV	10–100.0 μM	N-HCSs	3.0 μM	River and tap water	27
CPE	DPV	10–155.0 μM	Magnetic bar/DPSPP/RGO/Fe_3O_4 NPs	3.4 μM	River water	35
CPE	SWV	0.5–180 μM	*p*-Aminophenol	0.15 μM	Tap, well and river water	36
CPE	CV	5–43 μM	HAO/ZnO NPs	NR	N/A	55
CPE	SWV	0.9–400 μM	Benzoylferrocene carbon nanotube	0.1 μM	Tap, drinking and river water	37
CPE	SWV	0.5–250 μM	1,1-Bis(phenyl acetyl) ferrocene/NiO/CNTs	0.2 μM	Tap, well, river and wastewater	38
CPE	SWV	0.09–650 μM	Acetylferrocene/CdO NPs	0.06 μM	Tap, well, river and wastewater	20
CPE	DPV	1–400 μM	Quinizarine/TiO_2 nanoparticles	0.173 μM	Tap and well water	19
CPE	DPV	0.09–350 μM	DMBQ/ZnO/CNTs	0.04 μM	Tap, well, river, waste and boiler water	39
CPE	Amperometry	2.5–400 μM	Ni(II)-baicalein-MWCNT	0.6 μM	River and drinking water	81
CPE	SWV	0.05–500 μM		15.0 nM	Tap, well and river water	82

Table 1 (*Contd.*)

Electrode material	Detection method	Dynamic range	Electrode modification	Limit of detection	Sample medium	Reference
			2,7-Bis(ferrocenyl ethyl) fluoren-9-one			
CPE	SWV	1.1172.0 μM	*p*-Chloranil/CNTs	0.08 μM	Tap, well, river and wastewater	41
Graphene PE	SWV	2.0×10^{-7} to 2.5×10^{-4} M	2,7-Bis(ferrocenyl ethynyl) fluoren-9-one (2,7-BFE)	9.0×10^{-8} M	Tap, well and river water	42
CPE	DPV	0.1–500.0 μM	2PHC/ionic liquid/MWCNT	52 nM	Tap and river water	83
CPE	DPV	0.06–240.0 μM	La_2O_3/Co_3O_4 nanocomposite and ionic liquid	3.0 nM	Tap, well and river water	47
CPE	DPV	0.5–850.0 μM	CHIT-TiO_2	0.08 μM	Tap, well and wastewater	62
CPE	DPV and amperometry	20–7000 μM	CuO/ZSM-5 NPs	3.2 μM	Tap and river water	45
CPE	SWV	5–600 μM	MBIZBr/$CoFe_2O_4$ NPs	1 μM	Drinking, well, river and wastewater	46
CPE	SWV	0.025–10 μM	3,4′-AA/GO	0.012 μM	Tap, well and river water	48
Pencil GE	DPV	0.05–40 mM	Poly (cysteine)	48 μM	Tap and lake water	84
Pencil GE	DPV	0.5–167.42 mM	2-Amino-5-mercapto-1,3,4-thiadiazole	0.82 mM	Tap and river water	85
Carbon cloth electrode	Amperometry	0.1–692.2 μM	HZIF-Mo/PEDOT	0.04 μM	Ground, pond, deionised and drinking water	86
Poly(ethylene terephthalate) (PET) film	Amperometry	0.016–0.210 mM	Au NPs/SWCNT	0.72 μM	N/A	87
Graphite	Amperometry	0.8–100 μM	Fe_2O_3–$K_2Cu[Fe(CN)_6]$	0.5 μM	Tap, river and seawater	64
SPE	Amperometry	0.25–100.0 μM	$[(Cu(Ncp)_2]^{2+}$/Nf–MWCNT	0.08 μM	Tap bottled and lake waters; pharmaceutical sample	52
SPE	DPV	0.1–300.0 μM	TiO_2/GO	0.065 μM	Drinking, river and wastewater	61
SPE	DPV	1.0–125.0 μM	Fe_3O_4 NPs	0.4 μM	Well and river water	57
SPE	Amperometry	1.0–100.0 μM	ZnO/GR	0.5 μM	Tap and river water	56
SPE	Amperometry	0.01–560 μM	Au NPs@ quercetin carbon aerogels	0.003 μM	Industrial and sewage water	53
SPE	Amperometry	0.02 mM–7.0 mM	$RuIrO_x$/GO	1.6 μM	N/A	51
SPE	DPV	0.7–400.0 μM	$MoWS_2$ nano-composite	0.2 μM	Well and river water	88
SPE	DPV	0.09–375.0 μM	$MgAl_2O_4$	0.035 μM	Well and river water	63
SPE	DPV	0.007–385.0 μM	$NiCo_2O_4$/RGO	2.0 nM	Drinking, river and tap water	89

[a] Key: DPV: differential pulse voltammetry; CV: cyclic voltammetry; Au NPs: gold nanoparticles: MPTS: (3-mercaptopropyl)-trimethoxysilane; TAA: 2-mercapto-4-methyl-5-thiazoleacetic acid; PEDOT: poly(3,4-ethylenedioxythiophene); GO: graphene oxide; MWCNTs: multi-walled carbon nanotubes; LC: liquid chromatography; PEDOP: poly (3.4-ethylenedioxypyrrole); Pd NPs; palladium nanoparticles; NiHCF: nickel–cobalt hexacyanoferrate; CNTs: carbon nanotubes; Pt NPs: platinum nanoparticles; LSV: linear sweep voltammetry; SWCNTs: single-walled carbon nanotubes; CuTCPP: copper Tetrakis (4-carboxyphenyl) porphyrin; MMPF-6(Fe): metal–iron metalloporphyrin frameworks, $(Zr_6O_8(H_2O)_8(TCPP \cdot FeCl)_2)$DMBQ: 8,9-dihydroxy-7-methyl-12*H*-benzothiazolo[2,3-*b*]quinazolin-12-one; CTAB: cetyltrimethyl ammonium bromide; OAgNPs: oxadiazole self-assembled on silver nanoparticles; DPSPP: 1-[2,4-dihydroxy-5-(phenylazo-4-sulphonic acid)phenyl]-1-phenylmethanon; RGO: reduced graphene oxide; ZnO NPs: zinc oxide nanoparticles; NiO: nickel oxide; FNPs: [2-(4-((3-(trimethoxysilyl)propylthio)methyl)1-*H*1,2,3-triazol-1-yl)aceticacid]; 5-chloro, 2, 4-dihydroxyphenyl imidazo [4,5-*d*] [1,3] thiazin 7(3*H*)-one; CHIT: 3-(4′-amino-3′-hydroxy-biphenyl-4-yl)-acrylic acid (3,4-AA); MBIZBr: 1-methyl-3-butylimidazolium bromide; PHC: promazine hydrochloride; DMBQ: 8,9-dihydroxy-7-methyl-12*H*-benzothiazolo [2,3- *b*]quinazolin-12-one; HZIF: molybdum hybrid zeolitic imidazolate framework; oPMC: platelet ordered mesoporous carbon; 2PHC: 2-(4-oxo-3-phenyl-3,4-dihydroquinazolinyl)-*N*′-phenylhydrazinecarbothioamide; N-HCSs: nitrogen-doped hollow carbon spheres; $[(Cu(N_{cp})_2]^{2+}$: bis-neocuproine Cu(II) complex; Nf: Nafion; ZSM: zeolites.

$$\text{ARS (aq,red)} \rightarrow \text{ARS (aq,ox)} \quad (3)$$

$$2\text{ARS (aq,ox)} + 2NH_2OH \rightarrow 2\text{ARS (aq,red)} + N_2O + H_2O \quad (4)$$

This sensor was showed to report a LOD of 7.2 μM and was applied into the detection of hydroxylamine within spiked drinking and well water. Others have utilized Prussian blue,[17] anthio-quinazoline derivative,[18] quinizarine[19] and acetylferrocene,[20] all reporting wide dynamic ranges and low LODs. Baicalin, a flavonoid compound derived from the root of *Scutellaria baicalensis Georgi* has been utilized as the basis of an electrocatalytic sensor through adsorption on to MWCNTs, which were supported upon a GCE. As shown within Fig. 2A, the modified electrode exhibits a redox system attributed to the quinone–hydroquinone electrochemical reaction in the absence of hydroxylamine, but in the present a strong electrocatalytic response is observed.[21] There is no mention of any electrochemical mechanism in the authors work,[21] despite this, it was

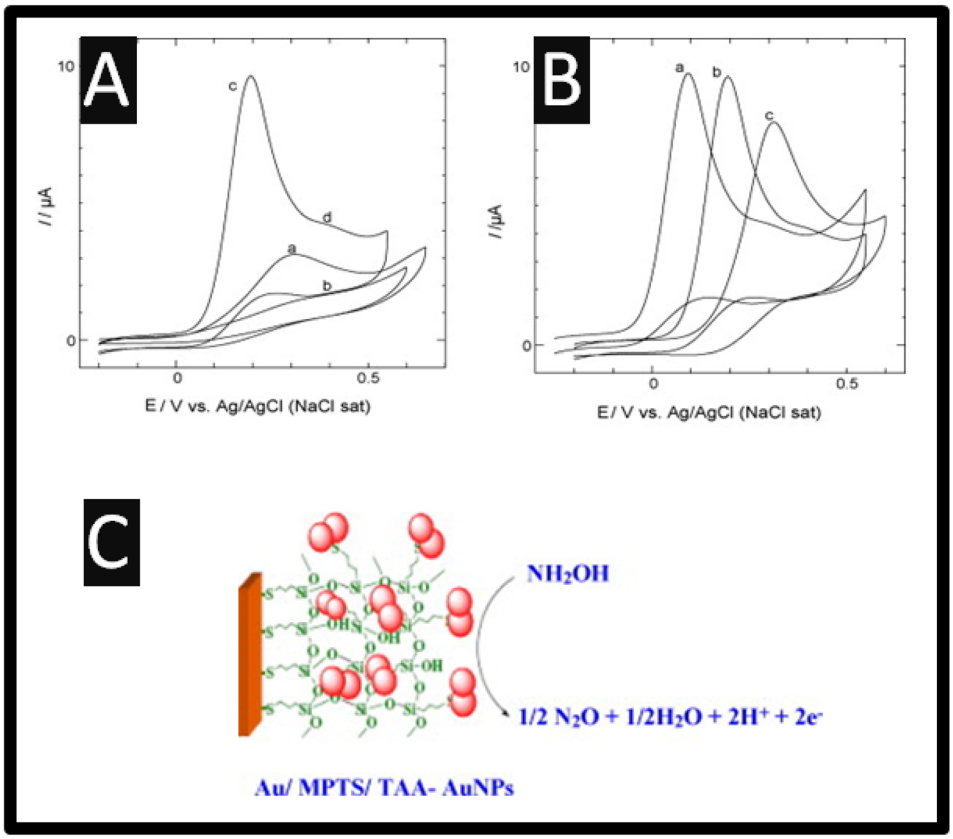

Fig. 1 (A) Cyclic voltammograms obtained for 0.50 mM hydroxylamine at (a) bare Au, (b) Au/MPTS, (c) Au/MPTS/TAA-AuNPs modified electrodes in 0.2 M PB solution (pH = 7.2) at a scan rate of 50 mV s^{-1}. (B) Cyclic voltammograms obtained for 0.50 mM hydroxylamine in 0.2 M PB solution (pH = 7.2) at a pH of 9.2 (a), 7.2 (b) and 5.2 (c). (C) An overview of the mechanism. Reprinted with permission from ref. 13. Copyright 2010 Elsevier.

shown that *via* the use of amperometry that a linear range of 0.5–400 μM with a LOD reported to be 0.1 μM which was shown to measure hydroxylamine within spiked tap water. The authors reported that this sensor offers a number of clear advantages, including a quick response time and an excellent limit of detection for hydroxylamine.[21] Based on the complexation interaction between Cu^{2+} and curcumin, and the π–π stacking interaction between curcumin and single-walled carbon nanotubes (SWCNTs), the authors have described a method to fabricate curcumin–Cu^{2+} complex (Cu^{2+}/CM/SWCNTs)-modified GC electrodes through straightforward immersion of the curcumin/SWCNTs (CM/SWCNTs)-modified GC electrodes into aqueous Cu^{2+};[22] please see Fig. 2B. In compared to the CM/SWCNTs-modified GC electrodes, the Cu^{2+}/CM/SWCNTs-modified GC electrode showed better stability and greater electrocatalytic performance towards the electrooxidation of hydroxylamine in physiological pH by taking advantage of the efficient electrocatalytic activity of curcumin–Cu^{2+} complex for hydroxylamine electrooxidation. The linear range was reported to be 1.0–100 μM and 100–1000 μM with a LOD of 0.019 μM. The repeatability and reproducibility of the electrochemical sensor was demonstrated through an RSD 4.6% for intra-electrode repeatability and RSD of 4.1% for inter-electrode reproducibility. With satisfactory results, the sensor was successfully used for selective hydroxylamine analysis in pharmaceutical samples, including hydroxyurea tables and pralidoxime iodide injections (PAM).[22]

Sudha *et al.*[23] reported a precipitation process to create copper oxide (CuO), cobalt oxide (Co_3O_4), and copper cobaltite ($CuCo_2O_4$). Through this a sensitive electrochemical sensor for hydroxylamine measurement has been developed; see Fig. 2C. The authors precipitation process making CuO, Co_3O_4, and $CuCo_2O_4$ have the morphologies and sizes of nanoflakes (300–350 nm), nanoplatelets (75–100 nm), and nanobricks (20–45 nm), respectively. Additionally, hydroxylamine is oxidized by CuO, Co_3O_4, and $CuCo_2O_4$ at +0.57 V, +0.53 V and, and +0.44 V, respectively. This sensor exhibited a linear range of 0.075 to 8.25 mM where they applied this for hydroxylamine detection in water samples in a very sensitive, selective, straightforward, approach. Other work has reported the use of C_{60}-functionalized CNTs modified with an ionic liquid (1-butyl-3-methylimidazolium tetrafluoroborate) nanocomposite for the simultaneous determination of hydrazine and hydroxylamine.[24] This sensor was prepared by simply casting MWCNTs with C_{60} in the ratio of 2 : 1. This sensor was able to measure hydrazine and hydroxylamine concentrations in the ranges of 0.05–700 and 1.0–300 μM, and the detection limits for hydrazine and hydroxylamine, were 17.2 and 28 nM respectively, while noting that there is a potential difference of ~450 mV between the two

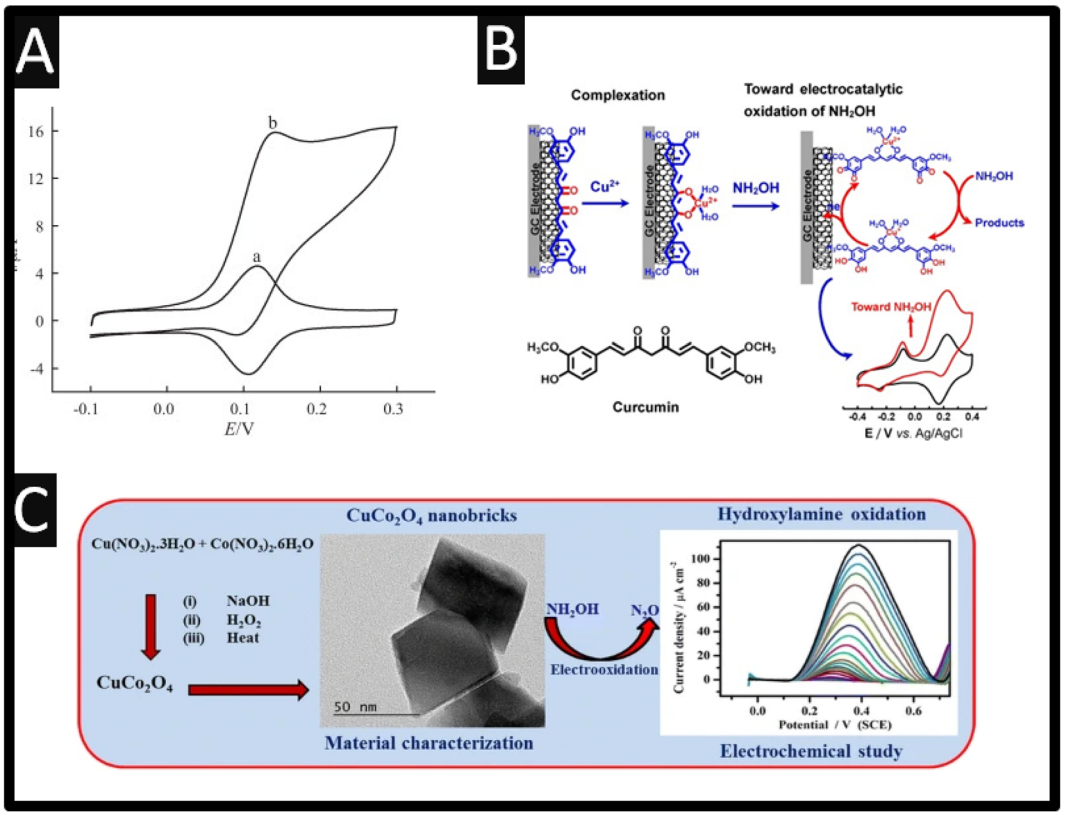

Fig. 2 (A) Cyclic voltammograms of a Baicalin/MWCNT/GCE in 0.1 M phosphate buffer (pH 7.0) in the absence (a) and presence (b) of 1.0 mM hydroxylamine, scan rate 5 mV s^{-1}. Reproduced from ref. 21. Copyright 2012 Elsevier. (B) As-synthesized $CuCo_2O_4$-nanobricks have been characterized by microscopic studies. Further, the $CuCo_2O_4$-nanobricks were used as catalyst to modify the GCE surface for sensing HA. In the sensing process, $CuCo_2O_4$-nanobricks modified electrode used as working electrode. Reproduced from ref. 23. Copyright 2019 Springer. (C) Schematic illustration of the preparation of curcumin–Cu^{2+}-based electrode and its electrocatalytic application toward electrooxidation of hydroxylamine. Reproduced from ref. 22. Copyright 2021 Elsevier.

peaks. This sensor was applied into spiked tap and auxiliary cooling water.

Of course, there are many reports that have utilized metal nanoparticles, please see Table 1. For instance, gold nanoparticles were easily absorbed into the cetyltrimethyl ammonium bromide (CTAB)/graphene oxide (GO) complex matrix when the film of the CTAB/GO complex was being produced directly on the GCE.[25] The use of GO is useful since it has negatively charged functional groups such as carboxylic groups and hydroxyl groups while CTAB is positively charged like all other quaternary ammonium salts. CTAB forms a stable surface complex with GO *via* the electrostatic interaction between the positively charged CTAB and negatively charged GO and the CTAB/GO complex presents unusual catalytic properties. The gold nanoparticles were modified *via* electrochemical deposition which has diameters in the range of 200–500 nm. When used as a sensor, a linear range of 10–1000 μM was reported with a LOD of 3.5 μM. The authors explored the spiked tap and lake water with recoveries in the range of 92–113%.

Other approaches use silver nanoparticles[26] due to their high conductivity, larger surface area, chemical stability, and access to fast electron transfer. The authors utilised silver nanoparticles formed *via* electrodeposition, onto which oxadiazole was self-assembled by immersing the modified electrode into a solution containing oxadiazole for 30 min. This sensor was applied to the sensing of hydroxylamine within spiked drinking and tap water. Of note is the use of immobilization of gold nanoparticles on metal–metalloporphyrin frameworks (AuNPs/MMPF-6(Fe)) through electrostatic adsorption.[25] The use of metal–organic frameworks (MOFs) represent an fascinating class of highly porous materials consisting of metal ions and organic ligands, but because of the poor conductivity of MOFs as well as the instability of MOFs structures in aqueous solutions, the fabrication of MOFs-based composites for electrochemical sensor applications is challenging. The authors overcome the limitations of MOFs through utilizing gold nanoparticles, which have a diameter of 15 nm. The mechanism is attributed to the redox couple of Fe(III)TCPP/Fe(II)TCPP in MMPF-6(Fe), which were promoted by the use of the gold nanoparticles. This sensor exhibited a dynamic range of 0.01 to 20 μM with a low LOD reported to be 4 nM. Another approach is the use of nitrogen-doped hollow carbon spheres (N-HCSs) for the sensing of hydroxylamine over the range 10 to 100 μM with a LOD reported to be 3 μM.[27] HCS are used in electrochemistry due to their reported properties which include low specific density, large specific surface area, admirable mechanical strength and reduced transport length for mass and charge transport.[27] The authors chose to utilize N-HCSs, where the use

of nitrogen is to increase the electrocatalytic behaviour of HCSs due to charge polarization and the difference in electronegativity and electron spin density between carbon and the nitrogen heteroatom. The authors utilized a silica template method to form the N-HCSs which have a diameter of 170 nm and successfully measured hydroxylamine within spiked river and tap water observing a recovery of 97–102.7%.

4. Carbon paste electrode based sensors

A unique type of heterogeneous carbon electrode known as a carbon paste electrode (CPE) is made of a mixture of carbon powder and a suitable water-immiscible or non-conducting binder.[28,29] Due to their reported benefits such as quick and simple surface renewal, low cost, large potential window, and easy preparation, CPEs are commonly used in both electrochemical investigations and electroanalysis.[30,31] Along with the aforementioned beneficial qualities and traits, the ability to incorporate additional ingredients during the paste preparation, creating what is known as a "modified carbon paste electrode," enables the creation of electrodes with the desired composition and properties.[32,33] As shown within Table 1, CPEs have been widely exploring as the sensor for hydroxylamine.

Early work on CPEs towards hydroxylamine was demonstrated by adding palladium powder into the carbon paste.[34] The electrocatalytic oxidation of hydroxylamine was discovered to involve electrogenerated palladium (0) at the electrode surface where the authors utilized a flow injection system with the CPE as an amperometric detector. A 4.0% relative standard deviation was seen after 60 times of repeated hydroxylamine injections (5 ng). A linear range between 0.1 and 10 ng of hydroxylamine was reported with a LOD corresponding to 20 pg. This methods was shown to sense hydroxylamine within spiked river water.[34]

Other approaches have utilized various mediators to give electrocatalytic responses compared to a bare CPE, which include a magnetic bar carbon paste electrode which was modified with 1-[2,4-dihydroxy-5-(phenylazo-4-sulphonic acid) phenyl]-1-phenylmethanon (DPSPP), reduced graphene oxide (RGO) and finally with iron oxide nanoparticles,[35] as well as a CPE that was chemically modified with multiwall carbon nanotubes (MWCNTs) and *p*-aminophenol,[36] and a benzoylferrocene modified carbon nanotube paste electrode,[37] and last a 1,1-bis(phenyl acetyl)ferrocene modified with NiO upon CNTs modified paste electrode.[38] Of note is the work which reports the sensing of hydroxylamine and thiosulfate using a acetylferroence–cadmium oxide nanoparticles within a CPE (AF/CdO/NPs/CPE).[20] Hydroxylamine and thiosulfate are two major compounds that are present in water and wastewater samples, and can be harmful to body health and thus the authors tackled this problem. The authors reported that the hydroxylamine electrochemical signal, at pH 7, it is altered by 430 mV using a AF/CdO/NPs/CPE compared to that observed at a CdO/NPs/CPE where the mediator (AF) has significantly improved the performance of the electrode toward hydroxylamine. The hydroxylamine and thiosulfate oxidation peak potentials are separated by around 340 mV. The calibration plot is also shown which gave a linear range from 0.09 to 650 μM and this sensor was shown to measure hydroxylamine within spiked tap, well, waste and river waters.[20] Related to the measurement of simultaneous analytes, a sensor has been reported for the sensing of hydroxylamine in the presence of phenol and sulfite in water and waste water samples.[39] This sensor was comprised of 8,9-dihydroxy-7-methyl-12*H*-benzothiazolo[2,3-*b*]quinazolin-12-one-ZnO/CNTs modified carbon paste electrode (DMBQ/ZnO/CNTs/CPE), which demonstrated resolution between the voltammetric peaks with anodic peaks at potentials of 160, 530 and 840 mV for hydroxylamine in the presence of phenol and sulfite respectively. This sensor was applied to the simultaneously measurements for hydroxylamine in the presence of phenol and sulfite within spiked tap, well, river, waste and boiler waters.[39]

Carbon nanotubes (CNTs) have attracted attention around the world and have significantly impacted a variety of applications.[40] Electrochemistry is one application where carbon nanotubes have proven their benefits, with uses including sensors and energy storage devices. In this connection, for the measurement of hydroxylamine in the presence of phenol, a carbon paste electrode modified with *p*-chloranil and CNTs was utilized.[41] A simultaneous assessment of hydroxylamine and phenol in mixtures is possible without major interferences thanks to the observed peak potential difference between hydroxylamine and phenol of 650 mV. The findings of the interference analysis show that the modified electrode has good selectivity for hydroxylamine and phenol and was applied to the sensing within spiked tap, well, river and waste waters.[41] Following the use of CNTs, a modified graphene paste electrode was created using a ferrocene derivative, 2,7-bis (ferrocenyl ethynyl) fluoren-9-one (2,7-BFE).[42] A linear range from 2.0×10^{-7} to 2.5×10^{-4} M was reported under optimal experimental conditions with the LOD being stated as 9.0×10^{-8} M. Ultimately, the hydroxylamine content of different (spiked) water samples was determined using this modified electrode.

One of the nanoporous materials that could serve as supports in various modified electrodes is zeolites.[43] Due to their characteristics, including their huge surface area, good size selectivity, and suitable pore-size distribution, zeolites—microporous aluminosilicate crystallites—have found extensive utility.[44] Moreover, compared to typical zeolites, nanozeolites, diameters below 100 nm, give rise to increased surface area and stronger catalytic activity. Rostami and co-workers[45] utilized a ZSM-5 zeolite featuring medium pores that range in size from 5.1 to 5.6 Å and three-dimensional channels made up of 10-membered rings, which were decorated with CuO. In their approach, ZSM-5 nanoparticles were fabricated *via* calcination, and CuO was loaded onto the ZSM-5 network where sodium ions were swapped for copper ions, achieved through vigorously shaking. This product was filtered, washed and then prepared by calcination. The sensor was employed for the simultaneous electrochemical oxidation of hydroxylamine and hydrazine using DPV; please see Fig. 3 for the proposed mechanisms. This sensor was shown that it can accurately determine the levels of

hydroxylamine and hydrazine in two samples of tap and river water while having an excellent RSD% (1.6–3.4) and excellent recoveries (94.1–106%).

Three significant water pollutants phenylhydrazine, phenol, and hydroxylamine are toxic to humans when present in the environment and in response, 1-methyl-3-butylimidazolium bromide (MBIZBr) and $CoFe_2O_4$ nanoparticles were mixed with graphite powder (MBIZBr/$CoFe_2O_4$ NPs/CPE) which was successfully employed as an amplification of a CPE.[46] As shown within Fig. 3, phenylhydrazine, phenol, and hydroxylamine present three separated oxidation signals with potentials ~313, ~618, and 927 mV, respectively. Also shown are the calibration plots for phenylhydrazine, phenol, and hydroxylamine. For completeness, the CPE sensor was applied in the measurement of phenylhydrazine, phenol, and hydroxylamine in water samples for its practical applicability.[46]

As a selective electrochemical sensor, a carbon paste electrode that had been chemically engineered with 3-(4′-amino-3′-hydroxy-biphenyl-4-yl)-acrylic acid (3,4′-AA) and with GO which was utilized to detect hydroxylamine.[48] The electrocatalytic oxidation current peak for hydroxylamine grew linearly with the concentration of hydroxylamine in the range of 0.025 to 10.0 μM where a LOD of 0.012 μM was reported. While the use of 3,4′-AA is evidently electrochemical active, in the presence of hydroxylamine the signal increased; the exact reason was not given. That said, the sensor was shown to measure hydroxylamine in spiked tap, river and well water samples.[48]

Using a CPE modified with La_2O_3/Co_3O_4 nanocomposite and ionic liquid (La_2O_3/Co_3O_4/IL/CPE), an effective, quick, and sensitive technique for the detection of hydroxylamine has been devised.[47] The sensor demonstrated good electrocatalytic activity and response capability for hydroxylamine where the authors showed that the electrochemical oxidation of hydroxylamine at the surface of La_2O_3/Co_3O_4/IL/CPE was 4.8 times greater than the signal at the surface of La_2O_3/Co_3O_4/CPE; the authors stating that the "IL is a good mediator".[47] Furthermore, the peak potential of hydroxylamine at the LaCo/IL/CPE surface was +700 mV (*vs.* Ag/AgCl), whereas hydroxylamine was not oxidized at the bare CPE until the potential reached +1200 mV (*vs.* Ag/AgCl); see Fig. 3. The authors also measured the diffusion coefficient of hydroxylamine which was reported to be 2.8 $\times 10^{-6}$ cm^2 s^{-1}. This sensor was able to measure hydroxylamine over the range 0.06–240 μM with a low reported LOD of 3 nM. Finally, the modified electrode was successfully used to quantify

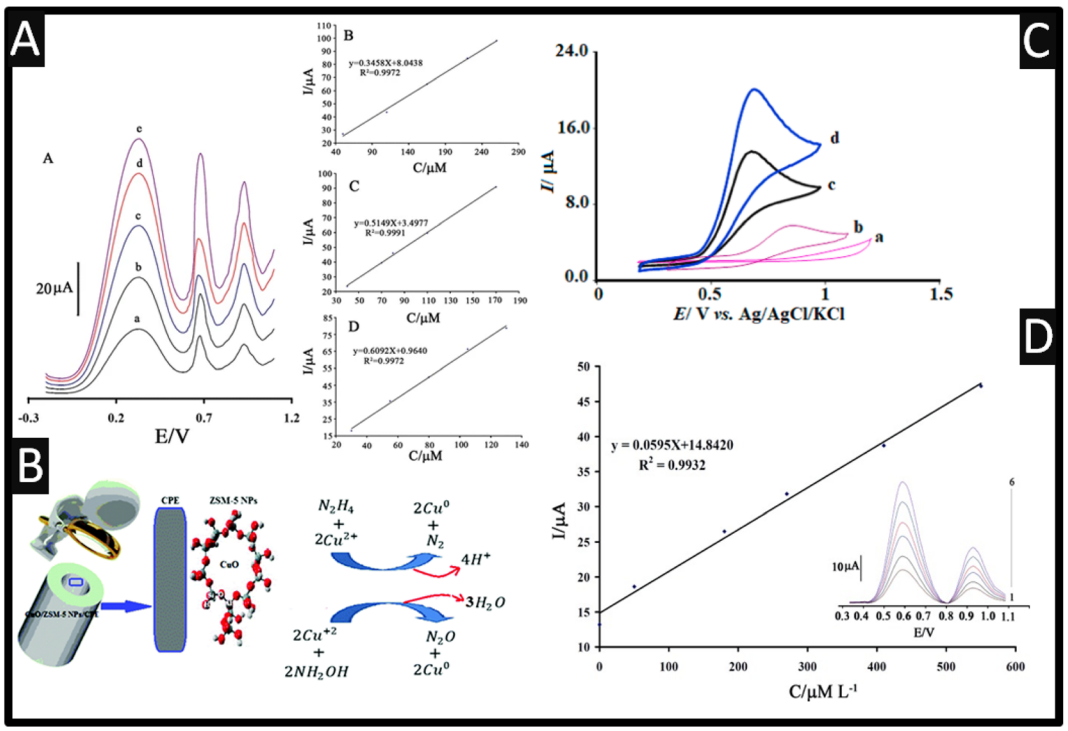

Fig. 3 (A) Insert: a square-wave voltammograms of MBIZBr/$CoFe_2O_4$ NPs/CPE at pH 8.0 containing different concentrations of phenylhydrazine, phenol, and hydroxylamine (from inner to outer) mixed solutions of (a) 50.0 + 40.0 + 30.0 μM, (b) 110.0 + 70.0 + 55.0 μM, (c) 165.0 + 80.0 + 80.0 μM, (d) 220.0 + 110 + 105.0 μM, and l 260.0 + 170.0 + 130.0 μM phenylhydrazine, phenol, and hydroxylamine, respectively. B Plot of the peak currents as a function of phenylhydrazine, concentration. C Plot of the peak currents as a function of phenol concentration. D Plot of the peak currents as a function of hydroxylamine concentration. Reproduced with permission from ref. 46. Copyright 2017 Springer. (B) Mechanism of simultaneous determination of hydrazine and hydroxylamine at CuO/ZSM-5 NPs/CPE. Reproduced with permission from ref. 45. Copyright 2017 The Royal Society of Chemistry. (C) The CVs of the unmodified CPE (a), the LaCo/CPE (b), the IL/CPE (c) and the LaCo/IL/CPE (d) in the presence of 100.0 μM HyA into 0.1 M PBS (pH of 7.0). Scan rate equalled 50 mV s^{-1} in all cases. Reprinted with permission from ref. 47. Copyright 2022 Elsevier. (D) The plots of the electrocatalytic peak current as a function of hydroxylamine concentration. Inset; SWVs of AF/CdO/NPs/CPE in 0.1 M PBS (pH 7.0) containing different concentrations of hydroxylamine-thiosulfate in μM. 1–6: 0.09 + 150.0; 50.0 + 200.0; 180.0 + 25.0; 270.0 + 300.0; 410 + 350 and 280.0 + 400.0, respectively. Reproduced with permission from ref. 20. Copyright 2015 Wiley.

the level of hydroxylamine in samples of well, tap, and river water.[47]

5. Screen-printed electrode-based sensors

Screen-printed electrodes (SPEs) are utilized as disposable electroanalytical sensors with the ability to be disposed of after use due to the economics of scale.[49] SPEs have several advantages over other electrodes, including low cost, mass production, disposability, miniaturization, lower sample consumption, compatibility with portable equipment, disposability and low background current, which can help them overcome their many drawbacks, including laborious cleaning processes and memory effects. However, thanks to their customizable surfaces, different sensing materials can perform better in terms of detection according to their improved surface properties. Due to their excellent electrocatalytic qualities, high stability, high surface-to-volume ratios, widespread availability, and fast electron transfer rates, nano-materials are utilized as modifiers in a variety of sensor and biosensor applications.[50] Among the materials most frequently utilized for electrode modification are metal nanoparticles, which have some really intriguing physicochemical features.

Sarno and Ponticorvo[51] have developed a novel approach to create a ruthenium–iridium oxide, supported upon graphene oxide ($RuIrO_x$ GO), nanohybrid which involved mixtures of salts of ruthenium and iridium within a solution (pH = 10), which was stirred for 1 h at 60° before calcination. As shown within Fig. 4A, a TEM is presented which shows the $RuIrO_x$ nanoparticles have an average diameter of 2.8 nm and are diffused on GO. The nanohybrid was used to simultaneously detect hydrazine (HY) and hydroxylamine (HA), which as shown in Fig. 4A, which shows good resolution (+0.36 V) and produced low detection limits of 2.1 μM and 1.6 μM for HY and HA, respectively.

The use of ZnO has been explored towards the sensing of hydroxylamine, such as being incorporated with MWCNTs,[39,54] and the hydroxylamine oxidase (HAO) enzyme.[55] For example, Nejad and co-workers[56] have utilized ZnO nanorods and graphene oxide nanosheets which were drop-casted onto SPEs. The sensors were able to measure over the range of 1.0 to 100.0 mM which reported a LOD of 0.5 mM. The authors demonstrated their sensor could measure hydroxylamine within spiked tap and river waters. SPEs have been decorated with Fe_3O_4 nanoparticles and utilized to measure hydroxylamine where the nanoparticle modified electrode was very effective in electrocatalysing the reaction.[57] The Fe_3O_4 nanoparticles were fabricated *via* a solvothermal process, but there was no characterization of the Fe_3O_4 nanoparticles. That said, the sensor was able to measure hydroxylamine over the range of 1–125 μM with a LOD reported to be 0.4 μM which they applied their sensors to measure within spiked well and river water.[57] This work has been extended to Fe_3O_4 nanoparticles functionalized by [2-(4-((3-(trimethoxysilyl)propylthio)methyl)1-*H*1,2,3-triazol-1-yl)aceticacid] (FNPs) and graphene oxide (GO)[58] and magnetic core–shell of Fe_3O_4@CuO[59] modified SPE with both sensors shown suitable responses when measurement of hydroxylamine within spiked tap, well and river samples.

Polypyrrole (Ppy) nanoparticles are popular due to their excellent electronic conductivity, high stability, simplicity of synthesis, and commendable biocompatibility. Also, the resonance of the delocalized electrons that are present throughout the entire carbon chain of the polymer structure is connected to their exceptional electrical capabilities. By modifying a SPE based on Ppy nanotubes (PpyNTs), Jahani *et al.*[60] have created an ultra-sensitive electroanalytical sensor for the detection of hydroxylamine. It was discovered that the PpyNTs/SPE was an effective platform for voltammetrically detecting hydroxylamine in a range from 0.005 to 290.0 mM with a LOD of 0.001 mM was reported. The newly designed sensor's significant capacity for detecting hydroxylamine in actual specimens is confirmed by the recovery rate of 96.7% to 104.3% in well and river water. Relating to the use of nanotubes, multiwalled carbon nanotube/SPEs modified with an efficient redox mediator of bis-neocuproine Cu(II) complex ($[(Cu(Ncp)_2]^{2+}$) can be used for the quick, selective, and sensitive detection of hydroxylamine using a flow injection analysis method.[52] Negatively charged Nafion (Nf) molecules and the $[(Cu(Ncp)_2]^{2+}$ complex were successively adsorbed onto MWCNT/SPCE through π–π stacking and electrostatic interactions, respectively, to create the modified electrode ($[(Cu(Ncp)_2]^{2+}$/Nf-MWCNT/SPE). As shown within Fig. 4B, a schematic representation of the proposed electrocatalytic oxidation mechanism is presented where the reversible oxidation of Cu(I)-Ncp to Cu(II) chelate complexes was responsible for the efficient redox pair seen in the cyclic voltammograms of the modified electrodes. Due to the synergistic interaction of MWCNT with the redox mediator, this redox couple demonstrated better electrocatalytic activity towards hydroxylamine in comparison to Nf-MWCNT/SPE and that of a bare SPE. The two electron oxidation of NH_2OH to N_2O, which is catalysed by $[(Cu(Ncp)_2]^{2+}$ as the redox mediator, is the mechanism responsible for the developed method's high sensitivity and selectivity.[52] The sensing of hydroxylamine was successfully evaluated with tap, bottle and lake waters and pharmaceutical samples.

As shown in Fig. 4C, carbon aerogels (CAs) with gold nanoparticles and quercetin (QCR) have been fabricated upon SPCEs ((AuNPs@QCR–CAs/SPE) which gave low detection limits towards HZ and HA.[53] In the fabrication of the sensor, a SPE electrode is modified with the carbon aerogel, which was fabricated *via* hydrothermal synthesis. Next a solution of quercetin was dissolved in sodium hydroxide with a gold salt to obtain the gold nanoparticles *via* electrodeposition. The authors found that the use of carbon aerogels with quercetin controlled the electrodeposition and provides gold nanoparticles in the range of 7–11 nm, attributed to the active interaction between the phenolic group of quercetin with the gold nanoparticles that are being formed during the electrodeposition procedure. This sensor was able to measure both HZ and HA, which exhibited peaks potentials of 0.05 and 0.16 V with linear ranges of 0.015–605 μM and 0.01–560 μM and a LODs of 0.005 and 0.003 μM respectively. Also shown within

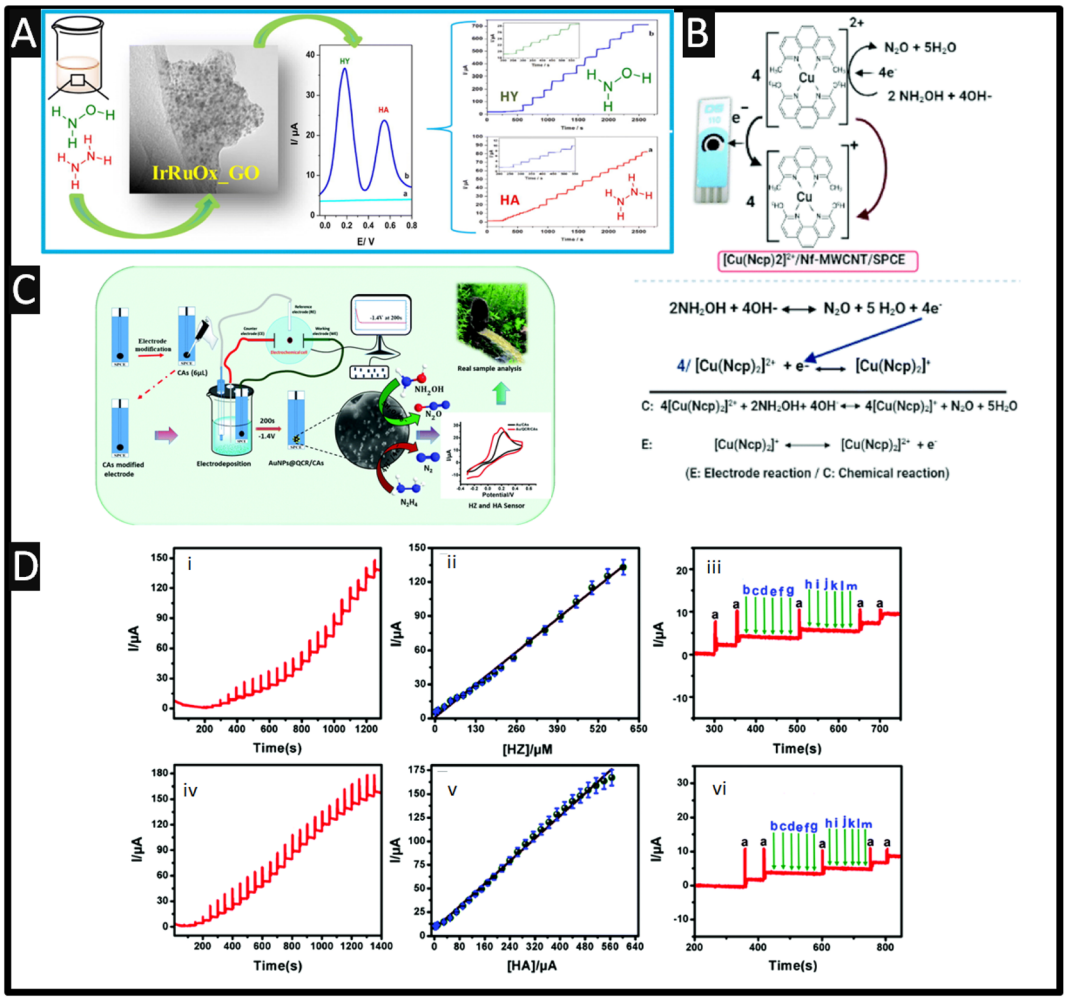

Fig. 4 (A) Differential pulse voltammetry of $RuIrO_x$_GO nanohybrid in PBS, without (cyan) and with (blue) hydrazine (0.3 mM) and hydroxylamine (0.5 mM), recorded at a scan rate of 0.04 V s^{-1}. (For interpretation of the references to color in this figure legend, the reader is referred to the web version of this article.) Also shown is the TEM images of $RuIrO_x$_GO nanohybrids as well as the amperometric responses of the $RuIrO_x$_GO nanohybrid after successive addition of (a) hydrazine at 0.18 V and (b) hydroxylamine at 0.54 V in a stirred PBS. Reprinted with permission from ref. 51. Copyright 2019 Elsevier. (B) A schematic representation of the proposed electrocatalytic oxidation mechanism of NH_2OH at $[Cu(Ncp)_2]^{2+}$/Nf–MWCNT/SPE in basic medium. Reproduced with permission from ref. 52. Copyright 2021 The Royal Society of Chemistry. (C) Schematic of carbon aerogel-modified AuNPs@quercetin *via* an environmentally benign method for the detection of environmental pollutants. (D) Chronoamperometry responds at AuNPs@QCR–CAs/SPE for different hydrazine (i) and hydroxylamine (iv) concentrations in the pH 7.0 PBS, the corresponding calibration curve for HZ (ii) and HA (v). Amperometric interferences response at AuNPs@QCR–CAs/SPE in the presence of 10 μM HZ (iii (a)) and 10 μM HA (vi (a)) with addition of different interferences (b) dopamine, (c) glucose, (d) fructose, (e) lactose, (f) sucrose, (g) ascorbic acid (h) Br^-, (i) I^-, (j) NO^-_3, (k) Zn^{2+}, (l) Sr^{2+}, (m) K+ respectively. Reproduced with permission from ref. 53. Copyright 2020 The Royal Society of Chemistry.

Fig. 4D are the chronoamperometry responses of the sensor towards hydrazine and hydroxylamine, corresponding calibration curves and also the response to interferents which shown no response; the authors attributed their sensor have proved the excellent conductivity, strong electroactive molecules adsorption and superficial electron transfer behaviour at AuNPs@QCR–CAs/SPE.[53]

TiO_2 has undergone substantial research in the recent years due to its remarkable optical, physiochemical, and electrical characteristics, which make it useful for a variety of applications. It has excellent catalytic behaviour in the reduction of various smaller organic compounds and is chemically stable in alkaline acidic solutions. TiO_2 is one of the most flexible and adaptable nanoparticles and has been used for hybridizing with graphene oxide, according to these benefits. In this direction, Malakootian and co-workers[61] have modified the SPE with graphene oxide and TiO_2 nanoparticles for the measurement of hydroxylamine which reported a linear range of 0.1–300 μM and a LOD reported to be 0.065 μM. This has been extended to quinizarine-TiO_2 nanoparticles modified carbon paste electrodes,[19] and a imidazole derivative-TiO_2 nanoparticle carbon paste sensor.[62]

Magnesium aluminate spinel, $MgAl_2O_4$, is a common perovskite material that exhibits excellent thermal shock resistance, a high melting point, a long energy band gap, outstanding mechanical strength, a high electrical resistance, and admirable

electrochemical properties. As a result, they are used for a variety of reasons and have multiple applications, including buffer layers for the formation of oxide superconductors, lightweight armor, ferroelectric random-access memory, high energy laser windows, and other uses. A sensitive electrochemical sensing system based on SPE modified with $MgAl_2O_4$ was constructed, its electrochemical performance was assessed, and it was then used to detect hydroxylamine in spiked well and river samples. The innovative aspect of the current work is the use of $MgAl_2O_4$ nanoparticles, which have outstanding catalytic activity and are being used for the first time to detect hydroxylamine which were fabricated *via* calcination process.[63] Clearly from this section it can be observed that the use of SPEs provides a good foundation to "electrically wiring" the electrode modification which includes portability, affordability, and simplicity towards the sensing of hydroxylamine.

6. Conclusion and outlook

We have overviewed the electroanalytical sensing of hydroxylamine where there is a vast approach of utilising a range of nanomaterials and electrocatalytic compounds. The majority of the electrochemical sensors are able to measure hydroxylamine over the low micromolar range with LODs reported to be nanomolar. These performances are comparable to other methods for the detection of hydroxylamine such as high-performance liquid chromatography, gas chromatography, chemiluminescence, and spectrophotometry but the ability of electroanalysis provides a portable, economical, yet sensitivity and selective approach for the sensing of hydroxylamine. One aspect that future researchers need to focus on is the choice of sample. As shown within Table 1 there is an extensive look at sensing hydroxylamine with water samples with select others measuring within pharmaceuticals. More focus should be on the sensing of hydroxylamine, such as measurement within seawater[64] and the direct comparison to laboratory standards to further validate their approach.

Author contributions

PSA: writing – review & editing; RDC: original draft, writing – review & editing. CEB: conceptualization, methodology, resources, formal analysis, writing – original draft, validation, writing – review & editing.

Conflicts of interest

There are no conflicts to declare.

References

1 W. P. Jencks, *Catalysis in Chemistry and Enzymology*, Courier Corporation, 1987.
2 P. Gross and R. P. Smith, *CRC Crit. Rev. Toxicol.*, 1985, **14**, 87–99.
3 A. Soler-Jofra, J. Pérez and M. C. M. van Loosdrecht, *Water Res.*, 2021, **190**, 116723.
4 *I. Guideline*, 2014.
5 C. Zhao and J. Song, *Anal. Chim. Acta*, 2001, **434**, 261–267.
6 T. Kumar, N. Xavier and M. Ramya, *J. Chromatogr. Sci.*, 2018, **57**, 63–70.
7 M. Saqib, W. Gao, J. Lai, L. Qi, S. Majeed, M. R. H. S. Gilani and G. Xu, *Chem. Commun.*, 2015, **51**, 6536–6539.
8 D. S. Frear and R. C. Burrell, *Anal. Chem.*, 1955, **27**, 1664–1665.
9 J. P. Guzowski, C. Golanoski and E. R. Montgomery, *J. Pharm. Biomed. Anal.*, 2003, **33**, 963–974.
10 M. Heyrovský and S. Vavřička, *Collect. Czech. Chem. Commun.*, 1969, **34**, 1204–1216.
11 T. Nagai and T. Matsuda, *J. Electroanal. Chem. Interfacial Electrochem.*, 1980, **110**, 311–317.
12 M. A. Hasnat, Z. Mumtarin and M. M. Rahman, *Electrochim. Acta*, 2019, **318**, 486–495.
13 P. Kannan and S. A. John, *Anal. Chim. Acta*, 2010, **663**, 158–164.
14 L. Shi, T. Wu, P. He, D. Li, C. Sun and J. Li, *Electroanalysis*, 2005, **17**, 2190–2194.
15 X. Qi and R. P. Baldwin, *Electroanalysis*, 1994, **6**, 353–360.
16 M. M. Ardakani, M. A. Karimi, S. M. Mirdehghan, M. M. Zare and R. Mazidi, *Sens. Actuators, B*, 2008, **132**, 52–59.
17 N. Zhang, G. Wang, A. Gu, Y. Feng and B. Fang, *Microchim. Acta*, 2010, **168**, 129–134.
18 M. M. Aghayizadeh, N. Nasirizadeh, S. M. Bidoki and M. E. Yazdanshenas, *Int. J. Electrochem. Sci.*, 2013, **8**, 8848–8862.
19 M. Mazloum-Ardakani, H. Beitollahi, Z. Taleat and H. Naeimi, *Anal. Methods*, 2010, **2**, 1764–1769.
20 M. Shabani-Nooshabadi and F. Tahernejad-Javazmi, *Electroanalysis*, 2015, **27**, 1733–1741.
21 H. Zhang and J. Zheng, *Talanta*, 2012, **93**, 67–71.
22 W. Xi, J. Zhai, L. Tian, S. Zhou and Z. Zhang, *Microchem. J.*, 2021, **161**, 105792.
23 V. Sudha, K. Annadurai, S. M. S. Kumar and R. Thangamuthu, *Ionics*, 2019, **25**, 5023–5034.
24 M. Mazloum-Ardakani, A. Khoshroo and L. Hosseinzadeh, *Sens. Actuators, B*, 2015, **214**, 132–137.
25 Y. Wang, L. Wang, H. Chen, X. Hu and S. Ma, *ACS Appl. Mater. Interfaces*, 2016, **8**, 18173–18181.
26 M. Hajisafari and N. Nasirizadeh, *Ionics*, 2017, **23**, 1541–1551.
27 A. Basande and H. Beitollahi, *J. Mater. Sci.: Mater. Electron.*, 2023, **34**, 647.
28 I. Švancara, K. Vytřas, K. Kalcher, A. Walcarius and J. Wang, *Electroanalysis*, 2009, **21**, 7–28.
29 I. Švancara, K. Vytřas, J. Barek and J. Zima, *Crit. Rev. Anal. Chem.*, 2001, **31**, 311–345.
30 S. Tajik, H. Beitollahi, F. G. Nejad, M. Safaei, K. Zhang, Q. Van Le, R. S. Varma, H. W. Jang and M. Shokouhimehr, *RSC Adv.*, 2020, **10**, 21561–21581.
31 P. Tomčik, C. E. Banks, T. J. Davies and R. G. Compton, *Anal. Chem.*, 2004, **76**, 161–165.
32 M. Mazloum-Ardakani, H. Beitollahi, Z. Taleat and H. Naeimi, *Anal. Methods*, 2010, **2**, 1764–1769.
33 M. B. Gholivand, M. Shamsipur, S. Dehdashtian and H. R. Rajabi, *Mater. Sci. Eng. C*, 2014, **36**, 102–107.

34 X. Cai, K. Kalcher, J. Lintschinger, C. G. Neuhold, J. Tykarski and B. Ogorevc, *Electroanalysis*, 1995, **7**, 556–559.
35 A. Benvidi, S. Jahanbani, A. Akbari and H. R. Zare, *J. Electroanal. Chem.*, 2015, **758**, 68–77.
36 A. A. Ensafi, E. Heydari-Bafrooei and B. Rezaei, *Chin. J. Catal.*, 2013, **34**, 1768–1775.
37 M. M. Foroughi, H. Beitollahi, S. Tajik, M. Hamzavi and H. Parvan, *Int. J. Electrochem. Sci.*, 2014, **9**, 2955–2965.
38 F. Golestanifar, H. Karimi-Maleh, N. Atar, E. Aydoğdu, B. Ertan, M. Taghavi, M. L. Yola and M. Ghaemy, *Int. J. Electrochem. Sci.*, 2015, **10**, 5456–5464.
39 V. K. Gupta, H. Karimi-Maleh and R. Sadegh, *Int. J. Electrochem. Sci.*, 2015, **10**, 303–316.
40 X. Ji, R. O. Kadara, J. Krussma, Q. Chen and C. E. Banks, *Electroanalysis*, 2010, **22**, 7–19.
41 R. Sadeghi, H. Karimi-Maleh, M. A. Khalilzadeh, H. Beitollahi, Z. Ranjbarha and M. B. P. Zanousi, *Environ. Sci. Pollut. Res.*, 2013, **20**, 6584–6593.
42 S. Esfandiari Baghbamidi, H. Beitollahi and S. Tajik, *Ionics*, 2015, **21**, 2363–2370.
43 M. Noroozifar, M. Khorasani-Motlagh, R. Akbari and M. B. Parizi, *Biosens. Bioelectron.*, 2011, **28**, 56–63.
44 T. Rohani and M. A. Taher, *Talanta*, 2009, **78**, 743–747.
45 S. Rostami, S. Naser Azizi and S. Ghasemi, *New J. Chem.*, 2017, **41**, 13712–13723.
46 F. Karimi, A. Beheshti, V. K. Gupta and M. C. Langerodi, *Ionics*, 2018, **24**, 1497–1503.
47 M. Nazari, H. Asadollahzadeh, M. Shahidi, N. Rastakhiz and S. Z. Mohammadi, *Mater. Chem. Phys.*, 2022, **286**, 126209.
48 S. Z. Mohammadi, H. Beitollahi and M. Mousavi, *Russ. J. Electrochem.*, 2017, **53**, 374–379.
49 A. García-Miranda Ferrari, S. J. Rowley-Neale and C. E. Banks, *Talanta Open*, 2021, **3**, 100032.
50 R. D. Crapnell and C. E. Banks, *Microchim. Acta*, 2021, **188**, 1–23.
51 M. Sarno and E. Ponticorvo, *Electrochem. Commun.*, 2019, **107**, 106510.
52 S. Ayaz, Y. Dilgin and R. Apak, *New J. Chem.*, 2021, **45**, 9143–9151.
53 C. Rajkumar, R. Nehru, S.-M. Chen, H. Kim, S. Arumugam and R. Sankar, *New J. Chem.*, 2020, **44**, 586–595.
54 C. Zhang, G. Wang, M. Liu, Y. Feng, Z. Zhang and B. Fang, *Electrochim. Acta*, 2010, **55**, 2835–2840.
55 M. Mohammadian, L. Farzampanah, A. Behtash-oskouie, S. Majdi, G. Mohseni, M. Imandar and M. Negahdary, *Int. J. Electrochem. Sci.*, 2013, **8**, 11215–11227.
56 F. G. Nejad, H. Beitollahi and R. Alizadeh, *Anal. Bioanal. Electrochem.*, 2017, **9**, 134–144.
57 M. H. Hemmati and M.-S. Ekrami-Kakhki, *Anal. Bioanal. Electrochem.*, 2018, **10**, 439–449.
58 H. Tashakkorian, B. Aflatoonian, P. M. Jahani and M. R. Aflatoonian, *J. Electrochem. Sci. Eng.*, 2021, **12**, 71–79.
59 G. A. Mohammadi, H. Beitollahi, I. Sheikhshoaie, S. Tajik and M. R. Aflatoonian, *Int. J. Environ. Anal. Chem.*, 2021, 1–15, DOI: **10.1080/03067319.2021.1975691**.
60 P. Mohammadzadeh Jahani, H. Beitollahi and A. Di Bartolomeo, *Appl. Sci.*, 2022, **12**, 7485.
61 M. Malakootian, Z. Gholami and H. Mahmoudi-Moghaddam, *Int. J. Environ. Anal. Chem.*, 2021, **101**, 35–47.
62 M. Banaei, A. Benvidi, Z. Abassi, M. D. Tezerjani and A. Akbari, *Anal. Bioanal. Electrochem.*, 2019, **11**, 757–773.
63 R. Riahi, M. A. Taher and H. Beitollahi, *Int. J. Environ. Anal. Chem.*, 2022, 1–13, DOI: **10.1080/03067319.2022.2118587**.
64 V. M. Allibai Mohanan, A. Kacheri Kunnummal and V. M. N. Biju, *Microchim. Acta*, 2016, **183**, 2013–2021.
65 I. ul Haque and K. Bano, *ECS Trans.*, 2008, **6**, 57.
66 Y. Wu, K. Zhang, J. Xu, L. Zhang, L. Lu, L. Wu, T. Nie, X. Zhu, Y. Gao and Y. Wen, *Int. J. Electrochem. Sci.*, 2014, **9**, 6594–6607.
67 H. R. Zare, F. Chatraei and N. Nasirizadeh, *J. Braz. Chem. Soc.*, 2010, **21**, 1977–1985.
68 J. Li and X. Lin, *Sens. Actuators, B*, 2007, **126**, 527–535.
69 H. R. Zare, N. Nasirizadeh, H. Ajamain and A. Sahragard, *Mater. Sci. Eng. C*, 2011, **31**, 975–982.
70 E. Lee, M. S. Ahmed, J.-M. You, S. K. Kim and S. Jeon, *Thin Solid Films*, 2012, **520**, 6664–6668.
71 K. Deng, C. Li, X. Qiu, J. Zhou and Z. Hou, *J. Electroanal. Chem.*, 2015, **755**, 197–202.
72 J. Li, H. Xie and Y. Li, *J. Solid State Electrochem.*, 2012, **16**, 795–802.
73 J. Li and H. Xie, *J. Appl. Electrochem.*, 2012, **42**, 271–277.
74 J. Li and H. Xie, *Ionics*, 2013, **19**, 105–112.
75 H. Beitollahi, S. Tajik, S. Z. Mohammadi and M. Baghayeri, *Ionics*, 2014, **20**, 571–579.
76 X. Zhao, J. Bai, X. Bo and L. Guo, *Anal. Chim. Acta*, 2019, **1075**, 71–80.
77 S. Premlatha, M. Chandrasekaran and G. N. K. R. Bapu, *Sens. Actuators, B*, 2017, **252**, 375–384.
78 M. Mazloum-Ardakani, M. Maleki and A. Khoshroo, *J. Nanostruct.*, 2018, **8**, 350–358.
79 Y. J. Yang and W. Li, *Fullerenes, Nanotubes Carbon Nanostruct.*, 2018, **26**, 195–204.
80 W. Xi, J. Zhai, Y. Zhang, L. Tian and Z. Zhang, *Microchim. Acta*, 2020, **187**, 1–9.
81 Z. Li, *Adv. Mater. Res.*, 2013, **631**, 30–34.
82 H. M. Moghaddam, H. Beitollahi, S. Tajik, M. Malakootian and H. K. Maleh, *Environ. Monit. Assess.*, 2014, **186**, 7431–7441.
83 H. Beitollahi, S. Tajik, S. Jahani and H. Khabazzadeh, *Anal. Bioanal. Electrochem.*, 2017, **9**, 806–818.
84 R. G. Krishnan and B. Saraswathyamma, *Mater. Chem. Phys.*, 2021, **271**, 124880.
85 S. Antherjanam and B. Saraswathyamma, *Mater. Chem. Phys.*, 2022, **275**, 125223.
86 C. Liang, F. Zhang, H. Lin, C. Jiang, W. Guo, S. Fan and F. Qu, *Electrochim. Acta*, 2019, **327**, 134945.
87 M.-P. N. Bui, X.-H. Pham, K. N. Han, C. A. Li, E. K. Lee, H. J. Chang and G. H. Seong, *Electrochem. Commun.*, 2010, **12**, 250–253.
88 P. Mohammadzadeh Jahani, S. Tajik, H. Beitollahi, S. Mohammadi and M. Jafari, *Int. J. Environ. Anal. Chem.*, 2021, **101**, 225–236.
89 S. Tajik, H. Beitollahi, S. a. Ahmadi, M. B. Askari and A. Di Bartolomeo, *Nanomaterials*, 2021, **11**, 3208.

